BJR

https://doi.org/10.1259/bjr.20180601

Received: 06 July 2018 | Revised: 07 November 2018 | Accepted: 23 November 2018

Cite this article as:
Jones RM, Hynynen K. Advances in acoustic monitoring and control of focused ultrasound-mediated increases in blood-brain barrier permeability. *Br J Radiol* 2019; **92**: 20180601.

REVIEW ARTICLE

Advances in acoustic monitoring and control of focused ultrasound-mediated increases in blood-brain barrier permeability

[1]RYAN M JONES, PhD and [1,2,3]KULLERVO HYNYNEN, MSc, PhD

[1]Physical Sciences Platform, Sunnybrook Research Institute, Toronto, ON, Canada
[2]Department of Medical Biophysics, University of Toronto, Toronto, ON, Canada
[3]Institute of Biomaterials and Biomedical Engineering, University of Toronto, Toronto, ON, Canada

Address correspondence to: Ryan M Jones
E-mail: *rmjones@sri.utoronto.ca*

ABSTRACT

Transcranial focused ultrasound (FUS) combined with intravenously circulating microbubbles can transiently and selectively increase blood–brain barrier permeability to enable targeted drug delivery to the central nervous system, and is a technique that has the potential to revolutionize the way neurological diseases are managed in medical practice. Clinical testing of this approach is currently underway in patients with brain tumors, early Alzheimer's disease, and amyotrophic lateral sclerosis. A major challenge that needs to be addressed in order for widespread clinical adoption of FUS-mediated blood–brain barrier permeabilization to occur is the development of systems and methods for real-time treatment monitoring and control, to ensure that safe and effective acoustic exposure levels are maintained throughout the procedures. This review gives a basic overview of the oscillation dynamics, acoustic emissions, and biological effects associated with ultrasound-stimulated microbubbles *in vivo*, and provides a summary of recent advances in acoustic-based strategies for detecting, controlling, and mapping microbubble activity in the brain. Further development of next-generation clinical FUS brain devices tailored towards microbubble-mediated applications is warranted and required for translation of this potentially disruptive technology into routine clinical practice.

INTRODUCTION

Nearly two decades ago, it was discovered that low-intensity pulsed focused ultrasound (FUS) applied in the presence of intravenously circulating contrast agent microbubbles can temporarily and selectively increase blood–brain barrier (BBB) permeability in rabbits,[1] providing a window for targeted delivery of therapeutics into the brain. Extensive pre-clinical work has demonstrated that a wide range of agents can be delivered to brain parenchyma using this approach (*e.g.* rodent models),[2–8] and that various biological effects can result from FUS exposures with microbubbles but without additional agent delivery, including increased hippocampal neurogenesis,[9,10] the clearance of amyloid-beta plaque pathology,[11–13] as well as the stimulation of angiogenesis.[14] Multiple laboratories have obtained positive therapeutic outcomes in animal models of brain tumors (*e.g.* rat models),[7,15,16] Alzheimer's disease (AD; *e.g.* transgenic mouse models,[11–13,17] natural canine model of aging[18]) and Parkinson's disease (*e.g.* transgenic rodent models).[19–21] Based on the favorable safety profile of transcranial FUS-mediated BBB permeabilization observed in large animal experiments performed using a commercial brain system (*e.g.* non-human primate[22] and trans-human skull porcine[23] models), the first clinical trials in human subjects began at Sunnybrook Research Institute (Toronto, ON) in late 2015. Two separate safety trials have recently completed with this extracorporeal FUS device (30 cm diameter hemispherical phased array, 1024 elements, 220–230 kHz center frequency; ExAblate Neuro, InSightec, Ltd., Tirat Carmel, Israel); one for enhanced chemotherapy delivery to brain tumors (NCT02343991) and another in patients with early AD[24] (NCT02986932). A third safety trial in patients with amyotrophic lateral sclerosis (ALS) is currently ongoing (NCT03321487). Researchers in France have concurrently demonstrated that repeated ultrasound exposures with microbubbles in circulation using a device implanted within the skull (10 mm diameter unfocused single-element transducer, 1.05 MHz center frequency; SonoCloud, CarThera, Inc., Paris, France) is safe and well-tolerated in patients with recurrent glioblastoma[25]

(NCT02253212), and there is an ongoing trial in patients with mild AD using this invasive applicator (NCT03119961).

It has been known since the 1950's that ultrasound exposure to the brain can lead to increased BBB permeability, when Bakay et al noted regions of trypan blue extravasation at the periphery of FUS-induced lesions in cat brain.[26] Subsequent studies indicated that increases in BBB permeability can be achieved in the absence of tissue damage via high-intensity FUS alone (*i.e.* without circulating microbubbles), however the approach was found to be inconsistent and unpredictable.[27,28] Both thermal and non-thermal mechanisms were hypothesized to contribute to the FUS-mediated BBB permeabilization observed in these early studies.[27,28] It has since been demonstrated that the dose threshold for thermal-mediated increases in BBB permeability is above that for brain tissue damage.[29] More recently, inadvertent increases in BBB permeability have been observed in acute stroke patients following transcranial Doppler sonography without microbubbles,[30] presumably due to skull heating effects.[31]

Following the seminal work of Hynynen et al.[1] (*i.e.* frequency = 1.63 MHz frequency, peak negative pressure ≈ 1 MPa *in situ*, pulse length = 10 ms, pulse repetition frequency = 1 Hz, exposure duration = 20 s, bolus of 50 μl kg^{-1} Optison® microbubbles), a wide range of treatment parameters have been investigated for inducing transient increases in BBB permeability via FUS and microbubbles (*e.g.* see reviews for details).[32,33] With appropriate treatment parameters, which include factors related to the ultrasound pulsing scheme and microbubble administration protocol,[34–40] increased microvascular permeability can be achieved without evident tissue damage upon histological examination.[22,41,42] Under these conditions, barrier functionality is generally restored within a few hours[1,43,44] independent of the treatment volume.[45] However, unsuitable parameters can result in a lack of desired effect or, conversely, extended durations of increased BBB permeability (*e.g.* 3–5 days[46,47]), vascular damage[48,49] or substantial neuroinflammation.[40,50] Treatment parameter selection is complicated by the application of FUS exposures through the human skull, as it is difficult to predict the acoustic pressure levels in the brain due to substantial variations in skull transmission efficiency,[51–53] imperfect trans-skull focusing,[54] as well as the potential for standing wave formation within the skull cavity.[55,56] Furthermore, the local vascularity and resulting microbubble concentration differ considerably between brain structures, and are thought to impact the obtained biological outcomes.[22,57,58] These sources of variability, combined with the relatively narrow window of parameters for which increased BBB permeability can be achieved without causing apparent tissue damage,[22,41,42] necessitate the development of systems and methods for real-time treatment monitoring and control.

MRI is commonly used to assess the outcome of FUS procedures. For instance, gadolinium-based contrast-enhanced T_1-weighted sequences can detect changes in microvascular permeability, whereas T_2- and T_2*-weighted sequences can monitor for the presence of unwanted edema or hemorrhage induced by the sonications, respectively.[1,22,24] However, the potential for a delayed onset of increased BBB permeability following FUS exposures (*e.g.* 5–15 min post-sonication),[59] coupled with the low temporal resolution of MRI (acquisition times ≈ seconds-to-minutes) relative to the timescales over which the relevant ultrasound–microbubble–vessel interactions take place (microseconds-to-milliseconds), restricts the use of MRI to post-treatment evaluations in this context. Further, repeated gadolinium-based MRI contrast agent injections can lead to longlasting brain deposits depending on the class of contrast agent that is administered, which may pose a risk to patients.[60] MR-thermometry, which is routinely employed for online monitoring of thermal FUS brain treatments, has limited utility during FUS BBB permeabilization procedures as the macroscopic temperature elevations generated are insignificant.[1,23]

Since spectral characteristics of the acoustic emissions generated from ultrasound-stimulated microbubbles can uncover features of the underlying bubble oscillation dynamics, remote detection of these signals may provide a means of guiding microbubble-mediated FUS treatments. The acoustic signals detected during FUS exposures with microbubbles for increased BBB permeability have been identified as potential indicators of treatment outcome[41,42,61,62] and have since been investigated for online monitoring and control of the procedures.[63–68] Multielement detector arrays can provide spatial information regarding microbubble activity in the brain[69–76] that can be exploited for acoustic exposure level calibration,[74] and element-specific aberration corrections can be incorporated into the reconstruction process to improve image quality in transcranial scenarios.[70–72,77–79] This review gives a basic overview of the oscillation dynamics, acoustic emissions, and biological effects associated with ultrasound-stimulated microbubbles *in vivo*, and provides a summary of recent advances in acoustic-based strategies for detecting, controlling, and mapping microbubble activity in the brain during transcranial FUS procedures.

ACOUSTIC CAVITATION: DYNAMICS, EMISSIONS, AND BIOEFFECTS

Acoustic cavitation refers to the interaction of acoustic waves with gas or vapor-filled cavities. At sufficiently high rarefactional pressures, cavitation and its accompanying bioeffects can be induced directly within tissue[80] and the vasculature[81] through nucleation of bubbles from the absorbed gases present *in vivo* and subsequent interactions of the nucleated bubbles with the incident acoustic field. Alternatively, encapsulated microbubbles, long used as contrast agents in diagnostic ultrasound,[82] can be injected into circulation to provide additional cavitation nuclei and reduce cavitation thresholds within the vasculature.[83] Commercially available ultrasound contrast agents consist of an air or perfluorocarbon core coated with a protein, polymer, or phospholipid shell to increase stability (*i.e.* circulation lifetime) at the sizes (<10 μm) required for successful entry into systemic circulation upon intravenous injection.[84]

In the context of biomedical ultrasound, cavitation activity is commonly separated into two distinct phenomenological regimes. Bubbles driven acoustically at low pressure amplitudes undergo periodic, volumetric oscillations about their equilibrium state that are dominated by the compressibility of the

gas core, and under sufficient driving pressures non-spherical surface mode vibrations can develop. This type of bubble activity is often termed *stable cavitation*.[85] The biological effects on the vasculature induced by stable cavitation are mainly attributed to a combination of acoustic microstreaming of the medium surrounding the bubble, which can exert large shear stresses on nearby cells or vessel walls,[86] and stretching of the capillary vessel walls during the expansion and contraction states of the bubble oscillation.[87] In addition, acoustic radiation forces can promote the translation of bubbles toward vessel walls[88] and enhance the stresses experienced by nearby endothelial cells. These highly localized mechanical forces are thought to contribute to the ultrasound-triggered cell wall and vessel wall permeability observed in the presence of cavitating microbubbles,[89] and may also play a role in FUS-mediated increases in BBB permeability through transient widening of the tight junctions.[57,90] There is also evidence to suggest that bubbles undergoing stable oscillations can generate sufficient stresses to rupture capillaries.[87]

If the acoustic pressure is increased above a certain threshold value, bubbles can rapidly expand and violently collapse during the compression phase of the incident acoustic wave. Because the resulting chaotic collapse is dominated by the inertia of the surrounding liquid, this behavior is often referred to as *inertial cavitation*.[85] Inertial cavitation can generate shock waves, high-velocity liquid jets, as well as extreme thermodynamic conditions that can lead to chemical reactions as well as light production. Encapsulated microbubbles can also be disrupted through fragmentation[91] or due to the loss of shell material.[92] Inertial bubble collapse has been associated with several biological effects *in vivo*, including apoptosis,[93] tissue necrosis,[94] as well as blood vessel rupture.[49]

Bubbles scatter or reradiate pressure waves in response to ultrasound stimulation.[85] These acoustic emissions can be detected remotely using piezoelectric transducers, providing a method for monitoring cavitation non-invasively. The pressure waves emitted by a bubble undergoing stable and inertial cavitation have markedly different acoustical signatures, which is most evident from differences in the spectral frequency content of the two scenarios. Under sufficient driving pressure, a bubble undergoing stable cavitation within an ultrasound field can emit harmonics (*i.e.* $(n+1)f$; n = 1,2,3…) as well as subharmonics (*i.e.* $f/(n+1)$; n = 1,2,3…) and ultraharmonics (*i.e.* $(2n+1)f/2$; n = 1,2,3…) of the excitation frequency (f). Theoretical models have shown that subharmonic and ultraharmonic behavior can only exist when the driving pressure exceeds certain threshold values, both for free[95,96] and encapsulated[97] bubbles. For free bubbles, the threshold for the first subharmonic (*i.e.* $f/2$) is minimized when the bubble is driven at twice its resonance frequency (*i.e.* $f = 2f_0$). For encapsulated microbubbles, rapid changes in the nonlinear shell elasticity and viscosity are thought to contribute to the enhancement of subharmonic behavior.[97,98] Optical evidence suggests that the maximal subharmonic response from encapsulated microbubbles is obtained when $1.7f_0 < f < 2.4f_0$, depending on the bubble size and transmit pressure employed.[99] Non-spherical modes of oscillation may also contribute to nonlinear bubble emissions.[100] As the driving pressure is further increased and the inertial cavitation threshold is approached, broadband continuous noise, also visible to some extent during stable cavitation, becomes more prominent.[85] Spectral analysis of cavitation emissions can therefore be used to characterize aspects of the underlying bubble dynamics, and this approach is under investigation for FUS treatment monitoring and control.

CAVITATION DETECTION

Perhaps the most common acoustic-based method for detecting cavitation remotely is through the use of a single-element passive cavitation detector (PCD), namely, a receive-only transducer that is separate from the therapy applicator[81,94] (Figure 1a). With this approach, cavitation activity can be identified by an increase in the scattered signal in the time domain, or by changes in spectral content (*e.g.* harmonic, subharmonic, ultraharmonic, and broadband emission bands) in the frequency domain. The size, shape, and piezoelectric material of the detector can have a major impact on its spatial sensitivity profile and on the spectral frequency characteristics of the measured signals, and these factors should be carefully considered when interpreting acoustic emissions data.[103] For example, detectors made of piezoelectric polymers (*e.g.* polyvinylidene fluoride) typically provide a broader frequency response than those made of piezoelectric ceramics (*e.g.* lead zirconate titanate) with equivalent geometry, with the trade-off of reduced levels of sensitivity. Single-element passive cavitation detection is now a well-established technique that is widely employed in both research and clinical settings for monitoring cavitation activity during the application of FUS. The existing clinical transcranial FUS brain systems (ExAblate Neuro, InSightec, Ltd., Tirat Carmel, Israel) have incorporated single-element PCDs for improved treatment safety, with sonications terminated automatically if signatures of significant inertial cavitation activity are observed.[23,104]

Several pre-clinical studies on FUS-mediated increased BBB permeability have reported correlations between spectral characteristics of the acoustic emissions captured using a single-element PCD and the resulting treatment outc omes.[39,41,42,58,61,62,68,105–107] For example, it has been shown that increased vascular permeability can be achieved without detecting broadband emissions or red blood cell (RBC) extravasations,[41,42] both evidence of inertial cavitation activity. These initial studies also reported significant increases in the strength of harmonic signals when exposure levels resulting in increased BBB permeability were employed, suggesting that harmonic emissions may be a useful metric for indicating treatment progress. Numerous reports have since attempted to correlate aspects of measured cavitation emissions with the resulting biological effects in a retrospective fashion, including the magnitude of increased BBB permeability, the BBB closure time, as well as the presence/absence of damage.[39,58,61,62,68,105–107] For instance, exposure parameters that result in detectable broadband emissions are frequently associated with vascular, parenchymal, or neuronal damage.[22,41,42,61,63,65,66,105] However, some studies have suggested that the detection of low-level broadband noise does not always result in damage,[39,42,65,66] whereas in other cases RBC extravasations have been observed in the treated zone without detecting any significant wideband signals.[39,64] The feasibility

Figure 1. Various detector types used to monitor acoustic cavitation remotely. (a) Single-element PCD potted in the middle of a spherically curved therapy transducer (FUS Instruments, Inc., Toronto, ON). (b) 1D linear array aligned with a spherically curved therapy transducer[101] (© 2014 IEEE. Reprinted, with permission, from *IEEE Transactions on Ultrasonics, Ferroelectrics, and Frequency Control*). (c) Multifrequency sparse hemispherical transmit/receive ultrasound phased array clinical prototype.[74] (d) Sparse hemispherical receiver array integrated within a clinical MRI-guided FUS brain system[102] (© Institute of Physics and Engineering in Medicine. Reproduced by permission of IOP publishing. All rights reserved).

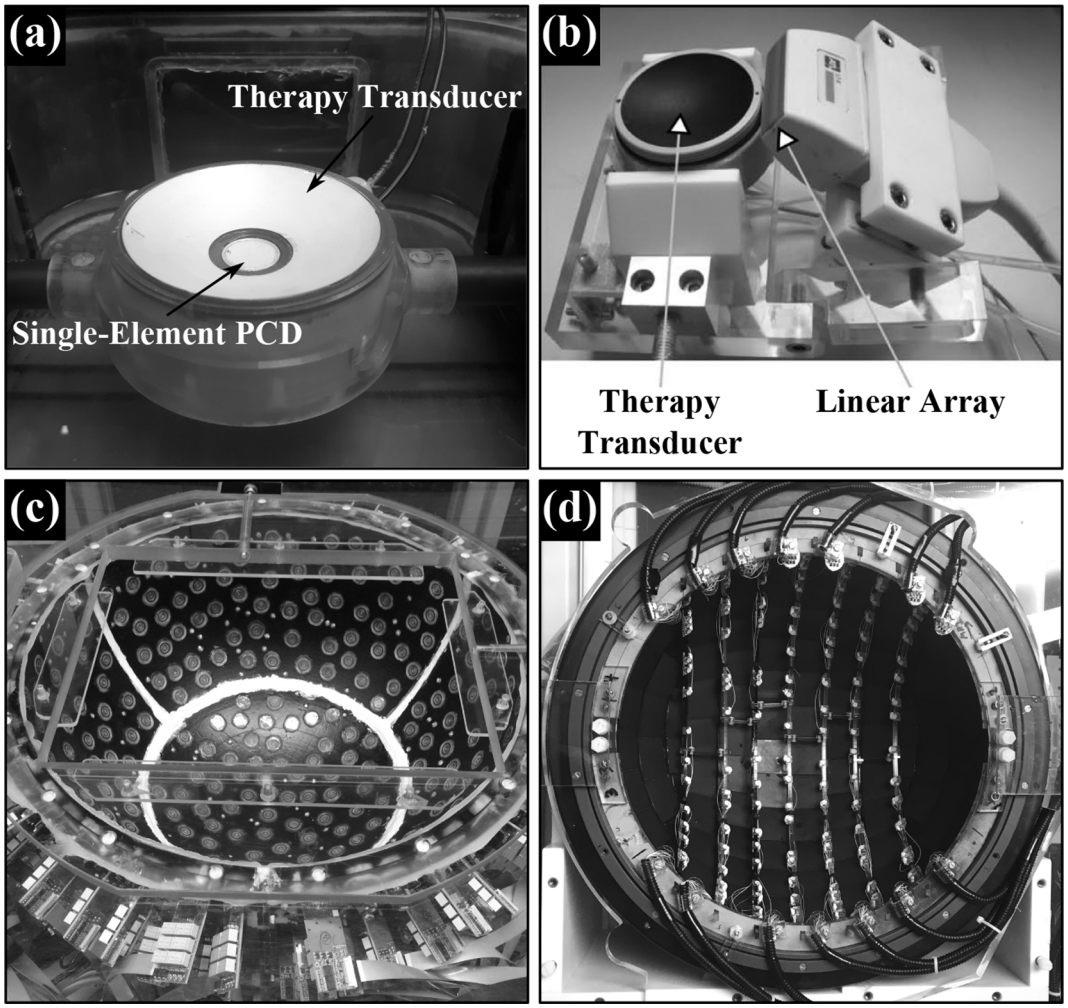

of monitoring contrast agent microbubble emissions transcranially with a single-element PCD has been demonstrated in large animal models through both primate[22,58] and human[23] skulls during pre-clinical testing of FUS-mediated increased BBB permeability, and initial clinical feasibility has recently been demonstrated.[24,108,109]

CAVITATION CONTROL

The retrospective studies described in the previous section have prompted research that has attempted to exploit the acoustic emissions detected during FUS-mediated increased BBB permeability for real-time treatment feedback to achieve the desired biological effects while preventing unwanted damage. In one study, Arvanitis et al[63] monitored changes in the combination of the first three harmonics of the transmit frequency during transcranial exposures in macaques using two separate detectors. The applied pressure level for each sonication was held constant, and was adjusted manually based on the spectral content of the received signals relative to baseline (*i.e.* without microbubbles in circulation) in previous exposures at the same target location for a given animal. The authors found that increasing the exposure level until a strong increase in harmonic emissions was detected relative to baseline, while staying below the threshold for substantial broadband noise, was an effective way of ensuring safe increases in BBB permeability. Expanding on this work, Sun et al[66] developed a closed-loop feedback controller that sustains increased levels of harmonic emissions and suppresses broadband noise, both relative to their respective baseline levels. This control paradigm has been shown to enable reliable delivery of pre-defined, therapeutically relevant drug concentrations in both healthy and tumor bearing rats without causing apparent tissue damage.

Tsai et al carried out constant pressure sonications in rodents with a confocal dual-frequency transducer setup designed to terminate exposures automatically if subharmonic emissions

were detected, and concluded that the detection of subharmonic activity was a good predictor of increased BBB permeability.[65] With the current implementation, this approach[65] lacks the flexibility to modulate the exposure level to account for variable *in situ* pressures within the brain. A recent pre-clinical study has proposed a closed-loop control scheme where a pre-determined level of ultraharmonic emissions is maintained throughout the entire exposure duration, however, safety assessments (*e.g.* histological examination) are necessary to determine whether this approach can lead to increased BBB permeability without causing tissue damage.[67] Finally, O'Reilly et al increased the transmit pressure incrementally on a burst-by-burst basis until either the first or second ultraharmonic signals were detected by a single sensor, at which point the pressure was reduced to a percentage of the value required to induce this microbubble activity for the remainder of the sonication.[64] In that study, sonications carried out at the 50% target level were shown to consistently produce safe increases in BBB permeability; lower target levels (*i.e.* 0 and 25%) were less likely to result in permeability enhancement, whereas at higher target levels (*i.e.* 75%) gross tissue damage was observed occasionally. Although ultraharmonics were analyzed in the original publication,[64] subsequent work has utilized subharmonic signals within the same general approach.[12] A modified version of this calibration method is currently being tested clinically during sonications in patients with early AD using a commercial transcranial FUS brain system.[24]

Although single-element PCDs can provide useful information for FUS treatment monitoring and control, the approach is limited by the sensor's fixed receive sensitivity profile, which inhibits spatially resolved cavitation detection from being carried out over an extended region. An inherent trade-off exists between the volume of sensitivity and spatial specificity of a single-element detector; focused receivers provide higher levels of sensitivity over a more confined spatial volume than do unfocused receivers of the same aperture size and spectral frequency characteristics. Focused detectors are therefore prone to missing cavitation events that originate from outside of their spatial sensing volume, whereas unfocused detectors cannot localize acoustic emissions with a high degree of spatial specificity and may fail to detect weaker cavitation events due to reduced levels of sensitivity. Unfocused detectors are thus more susceptible to false-positive detection events, such as the occurrence of cavitation activity in the coupling medium between the subject and the therapeutic transducer,[64] though it may be possible to ascertain whether or not acoustic emissions have originated from within the brain based on the relative spectral content of different non-linear frequency components.[110] Furthermore, when attempting to monitor cavitation activity in the brain, the location and orientation of the detector relative to the skull bone can greatly influence the nature of the recorded signals due to various effects such as local variations in attenuation, reflection/refractive effects, standing wave fields, and shear mode conversion.[52,56,111,112] Thus, despite their widespread use in pre-clinical and clinical settings, single-element PCDs suffer from a number of limitations, particularly when employed in transcranial scenarios.

CAVITATION MAPPING

Spatial information regarding microbubble activity would improve the safety of cavitation-mediated FUS procedures by allowing confirmation that the intended bioeffects are localized at the target(*s*) of interest while simultaneously monitoring for potential off-target microbubble behavior. During trans-skull FUS brain therapy, cavitation activity can be generated outside of the intended focal zone in sidelobes of the acoustic field[112] or as a result of intracranial reverberations,[55,56] and is more likely to occur in regions with a reduced cavitation threshold (*e.g.* tissue–ventricle interfaces).[113] Multiple pre-clinical studies have observed FUS-induced bioeffects outside of the intended treatment region following exposures with microbubbles in circulation,[112,114,115] including a recent study on FUS-mediated increased BBB permeability.[66] Mechanical translation and/or rotation of a single-element detector can enable spatial mapping of cavitation distributions,[116] though this approach requires highly stable cavitation fields over the course of signal acquisition and is impractical when such information is desired over large regions.

Pulse-echo imaging of ultrasound contrast agents via non-linear imaging sequences[117,118] or filtering techniques[119] can provide spatial information regarding microbubble activity *in vivo*. However, in the context of monitoring cavitation activity originating from within the brain, the acoustical properties (*e.g.* density, sound speed, attenuation) of human skull bone severely limit the use of typical B-mode frequencies.[51] The application of low frequencies and shear-mode conversion may provide a solution for bubble cloud imaging in patients in the future.[111,120]

Multielement passive sensor arrays can generate spatial information regarding source fields via beamforming of the acquired signals, and this approach has been utilized for a wide variety of applications in the field of acoustics.[121–125] Distribution of the receivers over a two-dimensional (2D) surface enables three-dimensional (3D) source field mapping.[122] Over the past decade, passive sensor arrays have become increasingly investigated within the therapeutic ultrasound community for spatial mapping of cavitation activity.[126–131] Passive acoustic imaging techniques have several important differences from traditional active imaging schemes (*e.g.* B-mode, Doppler) that make them particularly well-suited for ultrasound therapy guidance. Because passive imaging approaches rely on the therapy applicator for the excitation source, cavitation activity can be monitored continuously throughout the exposures without needing to gate the therapy burst to send interleaved imaging sequences. Passive beamforming methods typically form images based on correlations between the signals received on different elements of the array[125,128] without using absolute time-of-flight information (*n.b.* synchronized passive acoustic imaging has been achieved *in vitro*[101] and *in vivo*[73,76] using absolute time-of-flight information, and has been shown to improve the axial resolution of one-dimensional (1D) arrays when short excitation bursts are used), whereas traditional line-by-line active imaging exploits absolute time-of-flight to encode image depth. As a result, the spatial resolution obtained via conventional delay, sum, and integrate passive beamforming algorithms (*e.g.* see Refs. [71,125,128] for details) is

primarily dictated by the source's spectral characteristics and the receiver array's diffraction pattern, and, contrary to traditional active imaging schemes is independent of burst length.[129] This feature can be beneficial from a therapy monitoring perspective as it allows for continuous imaging throughout long therapy bursts without having to sacrifice spatial resolution. The use of long bursts also provides the opportunity to perform temporal averaging for improving the image signal-to-noise ratio (SNR) and temporal frequency resolution, the latter of which can aid in differentiating between specific types of cavitation activity, with the associated trade-off of reduced temporal resolution.[77] However, if the SNR of the individual detectors is sufficient, short-time analysis can provide spatial cavitation maps as a function of time within a given therapy burst at high temporal resolution. In the context of sonothrombolysis *in vitro* without exogenous cavitation nuclei, megahertz-rate processing has been shown to uncover details regarding the evolution of cavitation activity that can be missed when temporal averaging is carried out over the duration of ultrasound on-time.[132] Ultrafast 3D acoustic imaging has also been employed *in vivo* for spatiotemporal monitoring of contrast agent microbubbles during cavitation-mediated brain therapy.[133] In the future, high volume-rate 3D microbubble imaging is expected to aid in the development of FUS treatment control strategies,[74] and may also have application in bubble tracking for ultrasound angiography beyond the diffraction limit.[134,135]

The incorporation of passive acoustic imaging during cavitation-mediated FUS brain therapies would undoubtedly make the procedures more practical, however, ultrasound imaging in the human brain is complicated by the presence of the intervening skull. One approach to utilizing passive beamforming methods in the brain is to image through acoustic windows (*e.g.* temporal or suboccipital windows) using a narrow-aperture array, such as a 1D linear diagnostic probe[69,73,75,76,78] (Figure 1b). With this configuration, the local variations in skull morphology over the region of acoustic signal collection are small, and transcranial passive acoustic imaging can be achieved at sufficiently low frequencies without the need for element-specific aberration corrections on receive.[69,73,75,76,78] However, the limited range of acceptance angles from which source signals can be acquired using such a narrow-aperture device leads to poor spatial resolution, particularly in the axial direction (*i.e.* along the acoustic axis of the transducer), when employing delay, sum, and integrate passive beamforming methods.[71,125,128] Furthermore, the effective imaging region with a stationary small-aperture 1D receiver array is confined to a 2D area located near the central axis of the device. Lastly, considerable inter- and intrapatient variability exists in the availability of acoustic windows within human skull bone, and each acoustic window has a limited field-of-view within the brain.[136]

Alternatively, the use of large-aperture 2D receiver arrays allows source signals of interest to be acquired over a greater solid angle, and enables 3D acoustic imaging with improvements in spatial resolution, receive sensitivity, and the effective imaging volume during passive beamforming.[77] For monitoring cavitation activity within the brain in a clinical setting, the use of a receiver array covering the maximal available skull surface area would thus greatly improve upon the case of imaging through acoustic bone windows with a narrow-aperture device. Indeed, such a large-aperture design is employed in the transmit arrays that are currently used for transcranial FUS brain therapy in the clinic.[23,24] However, element-specific corrections will become necessary on receive to account for skull-induced aberrations, particularly at higher source frequencies, analogous to the case of transcranial transmit beam focusing with large-aperture arrays. It has been shown through both numerical simulations[77,78] and experimental measurements[70–72,79,134,137] that aberration corrections can provide improvements in image quality (*e.g.* positional error, main lobe volume, peak sidelobe ratio, image SNR) when employing passive acoustic imaging through human calvaria. Similar to the transmit focusing case, trans-skull aberration corrections can be obtained for imaging purposes through invasive measurements with an emitting/receiving transducer,[70,72] or via non-invasive approaches, such as CT-based ultrasound propagation modeling[71,77–79] or analysis of single bubble emissions originating from within the skull cavity.[134,137]

The FUS group at Sunnybrook Research Institute (Toronto, ON) has developed large-aperture transmit/receive hemispherical ultrasound arrays for microbubble-mediated transcranial therapy delivery and simultaneous 3D cavitation mapping.[70,72,74] Numerical simulations were carried out to inform the various device designs,[77] as transducer layout is known to play a major role in the obtainable transmit focusing quality and imaging point spread function of sparse array systems. In the initial work, O'Reilly et al integrated a sparse hemispherical receiver array within an existing fully populated transcranial phased array prototype.[70] Using this dual-mode system, the feasibility of 3D bubble cloud mapping in the brain during exposures carried out at pressure levels below and above the threshold for FUS-mediated increases in BBB permeability was demonstrated in rodents[70] with an intervening *ex vivo* human skullcap.[71] The same group has also fabricated multifrequency FUS brain prototype systems (Figure 1c) with increased flexibility from both therapy delivery and treatment monitoring standpoints.[72,74] Using one of these clinical-scale prototypes, it has been shown in both rabbits[74] and pigs[138] that 3D transcranial subharmonic imaging can be used to actively calibrate exposure levels for volumetric FUS-mediated increases in BBB permeability without causing apparent tissue damage (Figure 2). Researchers at Brigham and Womens Hospital (Boston, MA) have recently designed a sparse hemispherical array to fit within a clinical MRI-guided FUS brain system (Figure 1d), and have presented results of 3D bubble cloud mapping during non-thermal ablation in the brain of a macaque with this device.[102] A lab in Taiwan has also constructed a dual-mode ultrasound phased array system for microbubble-mediated FUS brain therapy.[139]

The continued development of systems and methods for transcranial therapy delivery and simultaneous 3D microbubble mapping/control are expected to improve the safety and efficacy of FUS-mediated BBB permeability enhancement procedures. Furthermore, as this general approach to treatment guidance is applicable to other cavitation-mediated therapies (*e.g.*

Figure 2. Example of 3D transcranial subharmonic microbubble imaging for calibrating acoustic exposure levels for inducing volumetric FUS-mediated BBB permeabilization in the thalamus of a New Zealand White rabbit (male, 3 kg) without causing apparent tissue damage. The data correspond to an animal from the "treatment group" of the study described in Ref.[74] (a) MRI data. (Left) Axial T_2w MR image acquired pre-FUS. Two non-overlapping target volumes (6 × 6 point grids, 1.0 mm point spacing, "*X*" symbol denotes calibration point) and their respective electronic beam steering trajectories are illustrated. (Center) Axial CE-T_1w MR image acquired immediately post-FUS. Regions of CE-T_1w MRI signal hyperintensity were induced by the exposures, indicating increased BBB permeability within the target volumes. (Right) Axial T_2*w MR image acquired 15 min post-FUS. No obvious regions of T_2*w MRI signal hypointensity were induced by the exposures. Histological examination of hematoxylin-eosin stained tissue sections revealed no RBC extravasations in this animal,[74] confirming that safe exposure levels were employed. Scale bar indicates 5 mm. (b) Ultrasound data corresponding to the posterior-most target volume (yellow). (Top Left) Estimated *in situ* spatial-peak temporal-peak negative pressure (p_{SPTPN}) and (Bottom Left) SPTA source field intensity of 3D acoustic reconstructions during a calibration sonication with microbubbles in circulation and subsequent therapeutic exposure at the 50% target level (f = 612 kHz, burst length = 10 ms, burst repetition frequency = 1 Hz). Baseline values from a pressure ramp at the same target location acquired without microbubbles in circulation are also shown. The received signals were captured using the array elements tuned to the subharmonic ($f/2$ = 306 kHz). A delay of 5 min between sonications allowed the bubbles to mostly clear from the circulation. (Top Right) Normalized MIP contour images (linear contours at 10% intervals) of temporal-average source field intensity volume distributions for the bursts 42 s (p_{SPTPN} = 0.59 MPa, no subharmonic activity) and 43 s (p_{SPTPN} = 0.60 MPa, subharmonic activity) into the calibration sonication. The imaging field-of-view is centered on the calibration point ("*X*" symbols). Scale bar indicates 3 mm. (Bottom Right) Frequency spectrum of the beamformed signal at the location of SPTA source field intensity for the bursts 42 and 43 s into the calibration sonication. The data are normalized to the spectral peak at the fundamental frequency for t = 43 s. Further details regarding the MRI and ultrasound protocols can be found in Ref.[74]

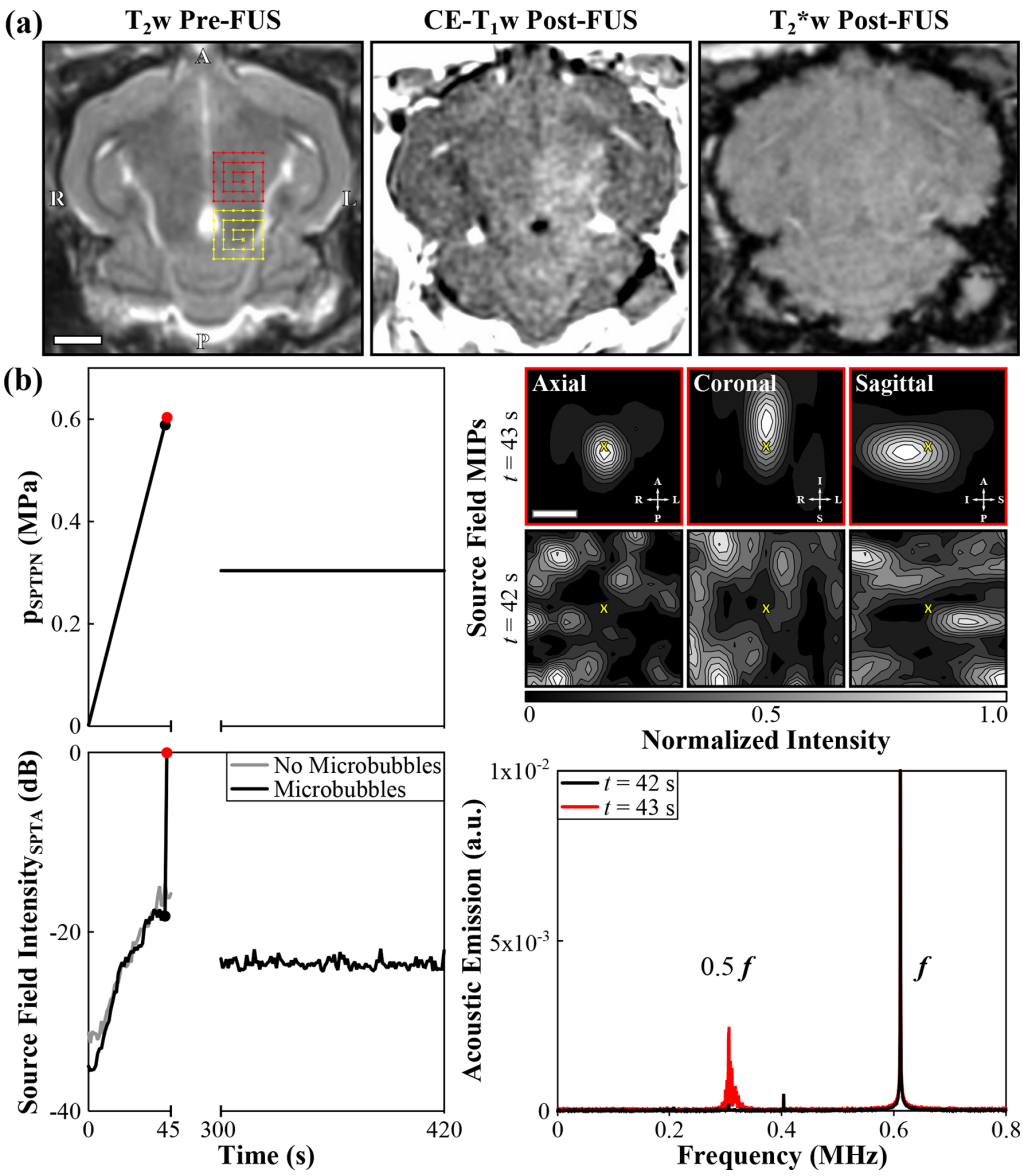

non-thermal ablation,[114,115] sonothrombolysis,[140] histotripsy[141]) and would improve upon existing cavitation monitoring strategies during treatments that are intended to be purely thermal-based,[53,104] these acoustic-based techniques stand to have a substantial impact on the clinical management of neurological disorders by making FUS brain interventions safe and practical.

CONCLUSION

Since the first pre-clinical experiments were published in 2001,[1] the application of transcranial FUS in conjunction with intravenously circulating microbubbles for increased BBB permeability has been shown by multiple independent laboratories to enable the delivery of a wide range of therapeutics into the brain and improve outcomes in various animal disease models—work that ultimately culminated in initial clinical testing in patients with brain tumors (in 2015), early AD (in 2017), and ALS (in 2018). Continual improvements in therapeutic ultrasound system capabilities and image-guidance strategies are expanding the use of FUS in the brain, thereby increasing the number of neurological indications for which FUS is a viable and effective treatment option. In particular, the development of next-generation clinical brain systems capable of transcranial therapy delivery and simultaneous detection, control, and mapping of microbubble activity will make FUS-mediated BBB permeability enhancement procedures more practical, and will help facilitate the technique's translation into routine clinical practice.

ACKNOWLEDGMENT

The authors would like to thank Meaghan O'Reilly and Dallan McMahon for proofreading the manuscript, as well as Calum Crake and Nathan McDannold for providing the image of their ultrasound system (Figure 1d).

CONFLICTS OF INTEREST

RMJ and KH are inventors on issued patents and patent applications related to transcranial focused ultrasound technology. KH owns stock in FUS Instruments, which has licensed IP related to the methods described in this review for pre-clinical use.

FUNDING

Financial support was provided by the National Institute of Biomedical Imaging and Bioengineering of the National Institutes of Health (R01 EB003268), the Canadian Institutes of Health Research (MOP 119312, FDN 154272), the W. Garfield Weston Foundation, and the Canada Research Chairs program.

CONFLICTS OF INTEREST

RMJ and KH are inventors on issued patents and patent applications related to transcranial focused ultrasound technology. KH owns stock in FUS Instruments, which has licensed IP related to the methods described in this review for pre-clinical use.

REFERENCES

1. Hynynen K, McDannold N, Vykhodtseva N, Jolesz FA. Noninvasive MR imaging-guided focal opening of the blood-brain barrier in rabbits. *Radiology* 2001; **220**: 640–6. doi: https://doi.org/10.1148/radiol.2202001804
2. Kinoshita M, McDannold N, Jolesz FA, Hynynen K. Noninvasive localized delivery of Herceptin to the mouse brain by MRI-guided focused ultrasound-induced blood-brain barrier disruption. *Proc Natl Acad Sci U S A* 2006; **103**: 11719–23. doi: https://doi.org/10.1073/pnas.0604318103
3. Burgess A, Ayala-Grosso CA, Ganguly M, Jordão JF, Aubert I, Hynynen K. Targeted delivery of neural stem cells to the brain using MRI-guided focused ultrasound to disrupt the blood-brain barrier. *PLoS One* 2011; **6**: e27877. doi: https://doi.org/10.1371/journal.pone.0027877
4. Baseri B, Choi JJ, Deffieux T, Samiotaki G, Tung Y-S, Olumolade O, et al. Activation of signaling pathways following localized delivery of systemically administered neurotrophic factors across the blood–brain barrier using focused ultrasound and microbubbles. *Phys Med Biol* 2012; **57**: N65–N81. doi: https://doi.org/10.1088/0031-9155/57/7/N65
5. Burgess A, Huang Y, Querbes W, Sah DW, Hynynen K. Focused ultrasound for targeted delivery of siRNA and efficient knockdown of Htt expression. *J Control Release* 2012; **163**: 125–9. doi: https://doi.org/10.1016/j.jconrel.2012.08.012
6. Etame AB, Diaz RJ, O'Reilly MA, Smith CA, Mainprize TG, Hynynen K, et al. Enhanced delivery of gold nanoparticles with therapeutic potential into the brain using MRI-guided focused ultrasound. *Nanomedicine* 2012; **8**: 1133–42. doi: https://doi.org/10.1016/j.nano.2012.02.003
7. Treat LH, McDannold N, Zhang Y, Vykhodtseva N, Hynynen K. Improved anti-tumor effect of liposomal doxorubicin after targeted blood-brain barrier disruption by MRI-guided focused ultrasound in rat glioma. *Ultrasound Med Biol* 2012; **38**: 1716–25. doi: https://doi.org/10.1016/j.ultrasmedbio.2012.04.015
8. Alkins R, Burgess A, Ganguly M, Francia G, Kerbel R, Wels WS, et al. Focused ultrasound delivers targeted immune cells to metastatic brain tumors. *Cancer Res* 2013; **73**: 1892–9. doi: https://doi.org/10.1158/0008-5472.CAN-12-2609
9. Scarcelli T, Jordão JF, O'Reilly MA, Ellens N, Hynynen K, Aubert I. Stimulation of hippocampal neurogenesis by transcranial focused ultrasound and microbubbles in adult mice. *Brain Stimul* 2014; **7**: 304–7. doi: https://doi.org/10.1016/j.brs.2013.12.012
10. Mooney SJ, Shah K, Yeung S, Burgess A, Aubert I, Hynynen K. Focused ultrasound-induced neurogenesis requires an increase in blood-brain barrier permeability. *PLoS One* **11**: e0159892. doi: https://doi.org/10.1371/journal.pone.0159892
11. Jordão JF, Thévenot E, Markham-Coultes K, Scarcelli T, Weng Y-Q, Xhima K, et al. Amyloid-β plaque reduction, endogenous antibody delivery and glial activation by brain-targeted, transcranial focused ultrasound. *Exp Neurol* 2013; **248**: 16–29. doi: https://doi.org/10.1016/j.expneurol.2013.05.008
12. Burgess A, Dubey S, Yeung S, Hough O, Eterman N, Aubert I, et al. Alzheimer disease in a mouse model: MR imaging-guided focused ultrasound targeted to the hippocampus opens the blood-brain barrier and improves pathologic abnormalities and behavior. *Radiology*

2014; **273**: 736–45. doi: https://doi.org/10.1148/radiol.14140245
13. Leinenga G, Götz J. Scanning ultrasound removes amyloid-β and restores memory in an Alzheimer's disease mouse model. *Sci Transl Med* 2015; **7**: 278ra33. doi: https://doi.org/10.1126/scitranslmed.aaa2512
14. McMahon D, Mah E, Hynynen K. Angiogenic response of rat hippocampal vasculature to focused ultrasound-mediated increases in blood-brain barrier permeability. *Sci Rep* 2018; **8**: 12178. doi: https://doi.org/10.1038/s41598-018-30825-8
15. Liu H-L, Hua M-Y, Chen P-Y, Chu P-C, Pan C-H, Yang H-W, et al. Blood-brain barrier disruption with focused ultrasound enhances delivery of chemotherapeutic drugs for glioblastoma treatment. *Radiology* 2010; **255**: 415–25. doi: https://doi.org/10.1148/radiol.10090699
16. Aryal M, Vykhodtseva N, Zhang YZ, Park J, McDannold N. Multiple treatments with liposomal doxorubicin and ultrasound-induced disruption of blood-tumor and blood-brain barriers improve outcomes in a rat glioma model. *J Control Release* 2013; **169**(1-2): 103–11. doi: https://doi.org/10.1016/j.jconrel.2013.04.007
17. Nisbet RM, Van der Jeugd A, Leinenga G, Evans HT, Janowicz PW, Götz J. Combined effects of scanning ultrasound and a tau-specific single chain antibody in a tau transgenic mouse model. *Brain* 2017; **140**: 1220–30. doi: https://doi.org/10.1093/brain/awx052
18. O'Reilly MA, Jones RM, Barrett E, Schwab A, Head E, Hynynen K. Investigation of the Safety of Focused Ultrasound-Induced Blood-Brain Barrier Opening in a Natural Canine Model of Aging. *Theranostics* 2017; **7**: 3573–84. doi: https://doi.org/10.7150/thno.20621
19. Samiotaki G, Acosta C, Wang S, Konofagou EE. Enhanced delivery and bioactivity of the neurturin neurotrophic factor through focused ultrasound-mediated blood--brain barrier opening *in vivo*. *J Cereb Blood Flow Metab* 2015; **35**: 611–22. doi: https://doi.org/10.1038/jcbfm.2014.236
20. Fan CH, Ting CY, Lin CY, Chan HL, Chang YC, Chen YY, et al. Noninvasive, targeted, and non-viral ultrasound-mediated GDNF-plasmid delivery for treatment of parkinson's disease. *Sci Rep* 2016; **6**: 19579. doi: https://doi.org/10.1038/srep19579
21. Mead BP, Kim N, Miller GW, Hodges D, Mastorakos P, Klibanov AL, et al. Novel focused ultrasound gene therapy approach noninvasively restores dopaminergic neuron function in a rat Parkinson's disease model. *Nano Lett* 2017; **17**: 3533–42. doi: https://doi.org/10.1021/acs.nanolett.7b00616
22. McDannold N, Arvanitis CD, Vykhodtseva N, Livingstone MS. Temporary disruption of the blood-brain barrier by use of ultrasound and microbubbles: safety and efficacy evaluation in rhesus macaques. *Cancer Res* 2012; **72**: 3652–63. doi: https://doi.org/10.1158/0008-5472.CAN-12-0128
23. Huang Y, Alkins R, Schwartz ML, Hynynen K. Opening the blood-brain barrier with MR imaging-guided focused ultrasound: preclinical testing on a trans-human skull porcine model. *Radiology* 2017; **282**: 123–30. doi: https://doi.org/10.1148/radiol.2016152154
24. Lipsman N, Meng Y, Bethune AJ, Huang Y, Lam B, Masellis M, et al. Blood-brain barrier opening in Alzheimer's disease using MR-guided focused ultrasound. *Nat Commun* 2018; **9**: 2336. doi: https://doi.org/10.1038/s41467-018-04529-6
25. Carpentier A, Canney M, Vignot A, Reina V, Beccaria K, Horodyckid C, et al. Clinical trial of blood-brain barrier disruption by pulsed ultrasound. *Sci Transl Med* 2016; **8**: 343re2. doi: https://doi.org/10.1126/scitranslmed.aaf6086
26. Bakay L, BALLANTINE HT, HUETER TF, Sosa D. Ultrasonically produced changes in the blood-brain barrier. *AMA Arch Neurol Psychiatry* 1956; **76**: 457–67. doi: https://doi.org/10.1001/archneurpsyc.1956.02330290001001
27. Vykhodtseva NI, Hynynen K, Damianou C. Histologic effects of high intensity pulsed ultrasound exposure with subharmonic emission in rabbit brain *in vivo*. *Ultrasound Med Biol* 1995; **21**: 969–79. doi: https://doi.org/10.1016/0301-5629(95)00038-S
28. Mesiwala AH, Farrell L, Wenzel HJ, Silbergeld DL, Crum LA, Winn HR, et al. High-intensity focused ultrasound selectively disrupts the blood-brain barrier *in vivo*. *Ultrasound Med Biol* 2002; **28**: 389–400. doi: https://doi.org/10.1016/S0301-5629(01)00521-X
29. McDannold N, Vykhodtseva N, Jolesz FA, Hynynen K. MRI investigation of the threshold for thermally induced blood-brain barrier disruption and brain tissue damage in the rabbit brain. *Magn Reson Med* 2004; **51**: 913–23. doi: https://doi.org/10.1002/mrm.20060
30. Reinhard M, Hetzel A, Krüger S, Kretzer S, Talazko J, Ziyeh S, et al. Blood-brain barrier disruption by low-frequency ultrasound. *Stroke* 2006; **37**: 1546–8. doi: https://doi.org/10.1161/01.STR.0000221813.27519.0b
31. Connor CW, Hynynen K. Patterns of thermal deposition in the skull during transcranial focused ultrasound surgery. *IEEE Transactions on Biomedical Engineering* 2004; **51**: 1693–706. doi: https://doi.org/10.1109/TBME.2004.831516
32. O'Reilly MA, Hynynen K. Ultrasound enhanced drug delivery to the brain and central nervous system. *Int J Hyperthermia* 2012; **28**: 386–96. doi: https://doi.org/10.3109/02656736.2012.666709
33. Aryal M, Arvanitis CD, Alexander PM, McDannold N. Ultrasound-mediated blood–brain barrier disruption for targeted drug delivery in the central nervous system. *Adv Drug Deliv Rev* 2014; **72**: 94–109. doi: https://doi.org/10.1016/j.addr.2014.01.008
34. McDannold N, Vykhodtseva N, Hynynen K. Use of ultrasound pulses combined with Definity for targeted blood-brain barrier disruption: a feasibility study. *Ultrasound Med Biol* 2007; **33**: 584–90. doi: https://doi.org/10.1016/j.ultrasmedbio.2006.10.004
35. McDannold N, Vykhodtseva N, Hynynen K. Effects of acoustic parameters and ultrasound contrast agent dose on focused-ultrasound induced blood-brain barrier disruption. *Ultrasound Med Biol* 2008; **34**: 930–7. doi: https://doi.org/10.1016/j.ultrasmedbio.2007.11.009
36. Chopra R, Vykhodtseva N, Hynynen K. Influence of exposure time and pressure amplitude on blood-brain-barrier opening using transcranial ultrasound exposures. *ACS Chem Neurosci* 2010; **1**: 391–8. doi: https://doi.org/10.1021/cn9000445
37. Choi JJ, Feshitan JA, Baseri B, Wang S, , Borden MA, Tung YS, et al. Microbubble-size dependence of focused ultrasound-induced blood-brain barrier opening *in* mice *in* vivo. *IEEE Trans Biomed Eng* 2010; **57**: 145–54. doi: https://doi.org/10.1109/TBME.2009.2034533
38. Choi JJ, Selert K, Gao Z, Samiotaki G, Baseri B, Konofagou EE. Noninvasive and localized blood-brain barrier disruption using focused ultrasound can be achieved at short pulse lengths and low pulse repetition frequencies. *J Cereb Blood Flow Metab* 2011; **31**: 725–37. doi: https://doi.org/10.1038/jcbfm.2010.155
39. McDannold N, Zhang Y, Vykhodtseva N. The effects of oxygen on ultrasound-induced blood-brain barrier disruption in mice. *Ultrasound Med Biol* 2017; **43**: 469–75. doi: https://doi.org/10.1016/j.ultrasmedbio.2016.09.019
40. McMahon D, Hynynen K. Acute inflammatory response following increased blood-brain barrier permeability induced by focused ultrasound is dependent on microbubble dose. *Theranostics* 2017; **7**:

3989–4000. doi: https://doi.org/10.7150/thno.21630
41. McDannold N, Vykhodtseva N, Hynynen K. Targeted disruption of the blood–brain barrier with focused ultrasound: association with cavitation activity. *Phys Med Biol* 2006; **51**: 793–807. doi: https://doi.org/10.1088/0031-9155/51/4/003
42. Tung Y-S, Vlachos F, Choi JJ, Deffieux T, Selert K, Konofagou EE. *In vivo* transcranial cavitation threshold detection during ultrasound-induced blood–brain barrier opening in mice. *Phys Med Biol* 2010; **55**: 6141–55. doi: https://doi.org/10.1088/0031-9155/55/20/007
43. Mei J, Cheng Y, Song Y, Yang Y, Wang F, Liu Y, et al. Experimental study on targeted methotrexate delivery to the rabbit brain via magnetic resonance imaging-guided focused ultrasound. *J Ultrasound Med* 2009; **28**: 871–80. doi: https://doi.org/10.7863/jum.2009.28.7.871
44. Marty B, Larrat B, Van Landeghem M, Robic C, Robert P, Port M, et al. Dynamic study of blood-brain barrier closure after its disruption using ultrasound: a quantitative analysis. *J Cereb Blood Flow Metab* 2012; **32**: 1948–58. doi: https://doi.org/10.1038/jcbfm.2012.100
45. O'Reilly MA, Hough O, Hynynen K. Blood-brain barrier closure time after controlled ultrasound-induced opening is independent of opening volume. *Journal of Ultrasound in Medicine* 2017; **36**: 475–83. doi: https://doi.org/10.7863/ultra.16.02005
46. Samiotaki G, Vlachos F, Tung Y-S, Konofagou EE. A quantitative pressure and microbubble-size dependence study of focused ultrasound-induced blood-brain barrier opening reversibility *in vivo* using MRI. *Magn Reson Med* 2012; **67**: 769–77. doi: https://doi.org/10.1002/mrm.23063
47. Samiotaki G, Konofagou EE. Dependence of the reversibility of focused- ultrasound-induced blood-brain barrier opening on pressure and pulse length *in vivo*. *IEEE Trans Ultrason Ferroelectr Freq Control* 2013; **60**: 2257–65. doi: https://doi.org/10.1109/TUFFC.2013.6644731
48. Miller DL, Quddus J. Diagnostic ultrasound activation of contrast agent gas bodies induces capillary rupture in mice. *Proc Natl Acad Sci U S A* 2000; **97**: 10179–84. doi: https://doi.org/10.1073/pnas.180294397
49. Aviv RI, Huynh T, Huang Y, Ramsay D, Van Slyke P, Dumont D, et al. An *in vivo*, MRI-integrated real-time model of active contrast extravasation in acute intracerebral hemorrhage. *AJNR Am J Neuroradiol* 2014; **35**: 1693–9. doi: https://doi.org/10.3174/ajnr.A3939
50. Kovacs ZI, Kim S, Jikaria N, Qureshi F, Milo B, Lewis BK, et al. Disrupting the blood-brain barrier by focused ultrasound induces sterile inflammation. *Proc Natl Acad Sci U S A* 2017; **114**: E75–E84. doi: https://doi.org/10.1073/pnas.1614777114
51. Fry FJ, Barger JE. Acoustical properties of the human skull. *J Acoust Soc Am* 1978; **63**: 1576–90. doi: https://doi.org/10.1121/1.381852
52. Pichardo S, Sin VW, Hynynen K. Multi-frequency characterization of the speed of sound and attenuation coefficient for longitudinal transmission of freshly excised human skulls. *Phys Med Biol* 2011; **56**: 219–50. doi: https://doi.org/10.1088/0031-9155/56/1/014
53. Schwartz ML, Yeung R, Huang Y, Lipsman N, Krishna V, Jain JD, et al. Skull bone marrow injury caused by MR-guided focused ultrasound for cerebral functional procedures. *J Neurosurg* 2018; **4**: 1–5. doi: https://doi.org/10.3171/2017.11.JNS17968
54. Pulkkinen A, Werner B, Martin E, Hynynen K. Numerical simulations of clinical focused ultrasound functional neurosurgery. *Phys Med Biol* 2014; **59**: 1679–700. doi: https://doi.org/10.1088/0031-9155/59/7/1679
55. Baron C, Aubry J-F, Tanter M, Meairs S, Fink M. Simulation of intracranial acoustic fields in clinical trials of sonothrombolysis. *Ultrasound Med Biol* 2009; **35**: 1148–58. doi: https://doi.org/10.1016/j.ultrasmedbio.2008.11.014
56. Song J, Pulkkinen A, Huang Y, Hynynen K, Pulkkinen A. Investigation of standing-wave formation in a human skull for a clinical prototype of a large-aperture, transcranial MR-guided focused ultrasound (MRgFUS) phased array: an experimental and simulation study. *IEEE Trans Biomed Eng* 2012; **59**: 435–44. doi: https://doi.org/10.1109/TBME.2011.2174057
57. Hosseinkhah N, Goertz DE, Hynynen K. Microbubbles and blood-brain barrier opening: a numerical study on acoustic emissions and wall stress predictions. *IEEE Trans Biomed Eng* 2015; **62**: 1293–304. doi: https://doi.org/10.1109/TBME.2014.2385651
58. Wu SY, Sanchez CS, Samiotaki G, Buch A, Ferrera VP, Konofagou EE. Characterizing focused-ultrasound mediated drug delivery to the heterogeneous primate brain in vivo with acoustic monitoring. *Sci Rep* 2016; **6**: 37094. doi: https://doi.org/10.1038/srep37094
59. Cho EE, Drazic J, Ganguly M, Stefanovic B, Hynynen K. Two-photon fluorescence microscopy study of cerebrovascular dynamics in ultrasound-induced blood-brain barrier opening. *J Cereb Blood Flow Metab* 2011; **31**: 1852–62. doi: https://doi.org/10.1038/jcbfm.2011.59
60. Gulani V, Calamante F, Shellock FG, Kanal E, Reeder SB, International Society for Magnetic Resonance in Medicine Gadolinium deposition in the brain: summary of evidence and recommendations. *Lancet Neurol* 2017; **16**: 564–70. doi: https://doi.org/10.1016/S1474-4422(17)30158-8
61. Yang FY, Fu WM, Chen WS, Yeh WL, Lin WL. Quantitative evaluation of the use of microbubbles with transcranial focused ultrasound on blood-brain-barrier disruption. *Ultrason Sonochem* 2008; **15**: 636–43. doi: https://doi.org/10.1016/j.ultsonch.2007.08.003
62. O'Reilly MA, Hynynen K. A PVDF receiver for ultrasound monitoring of transcranial focused ultrasound therapy. *IEEE Trans Biomed Engg* 2012; **57**: 2286–94. doi: https://doi.org/10.1109/TBME.2010.2050483
63. Arvanitis CD, Livingstone MS, Vykhodtseva N, McDannold N. Controlled ultrasound-induced blood-brain barrier disruption using passive acoustic emissions monitoring. *PLoS One* 2012; **7**: e45783. doi: https://doi.org/10.1371/journal.pone.0045783
64. O'Reilly MA, Hynynen K. Blood-brain barrier: real-time feedback-controlled focused ultrasound disruption by using an acoustic emissions-based controller. *Radiology* 2012; **263**: 96–106. doi: https://doi.org/10.1148/radiol.11111417
65. Tsai C-H, Zhang J-W, Liao Y-Y, Liu H-L. Real-time monitoring of focused ultrasound blood-brain barrier opening via subharmonic acoustic emission detection: implementation of confocal dual-frequency piezoelectric transducers. *Phys Med Biol* 2016; **61**: 2926–46. doi: https://doi.org/10.1088/0031-9155/61/7/2926
66. Sun T, Zhang Y, Power C, Alexander PM, Sutton JT, Aryal M, et al. Closed-loop control of targeted ultrasound drug delivery across the blood–brain/tumor barriers in a rat glioma model. *Proc Nat Aca Sci* 2017; **114**: E10281–E10290. doi: https://doi.org/10.1073/pnas.1713328114
67. Bing C, Hong Y, Hernandez C, Rich M, Cheng B, Munaweera I, et al. Characterization of different bubble formulations for blood-brain barrier opening using a focused ultrasound system with acoustic feedback control. *Sci Rep* 2018; **8**: 7986. doi: https://doi.org/10.1038/s41598-018-26330-7
68. Kamimura HAS, Flament J, Valette J, Cafarelli A, Aron Badin R, Hantraye P, et al.

Feedback control of microbubble cavitation for ultrasound-mediated blood–brain barrier disruption in non-human primates under magnetic resonance guidance. *Journal of Cerebral Blood Flow & Metabolism* 2018; **10**: 0271678X1775351. doi: https://doi.org/10.1177/0271678X17753514

69. Arvanitis CD, Livingstone MS, McDannold N. Combined ultrasound and MR imaging to guide focused ultrasound therapies in the brain. *Phys Med Biol* 2013; **58**: 4749–61. doi: https://doi.org/10.1088/0031-9155/58/14/4749
70. O'Reilly MA, Jones RM, Hynynen K. Three-dimensional transcranial ultrasound imaging of microbubble clouds using a sparse hemispherical array. *IEEE Trans Biomed Eng* 2014; **61**: 1285–94. doi: https://doi.org/10.1109/TBME.2014.2300838
71. Jones RM, O'Reilly MA, Hynynen K. Experimental demonstration of passive acoustic imaging in the human skull cavity using CT-based aberration corrections. *Med Phys* 2015; **42**: 4385–400. doi: https://doi.org/10.1118/1.4922677
72. Deng L, O'Reilly MA, Jones RM, An R, Hynynen K. A multi-frequency sparse hemispherical ultrasound phased array for microbubble-mediated transcranial therapy and simultaneous cavitation mapping. *Phys Med Biol* 2016; **61**: 8476–501. doi: https://doi.org/10.1088/0031-9155/61/24/8476
73. Burgess MT, Apostolakis I, Konofagou EE. Power cavitation-guided blood-brain barrier opening with focused ultrasound and microbubbles. *Phys Med Biol* 2018; **63**: 065009. doi: https://doi.org/10.1088/1361-6560/aab05c
74. Jones RM, Deng L, Leung K, McMahon D, O'Reilly MA, Hynynen K. Three-dimensional transcranial microbubble imaging for guiding volumetric ultrasound-mediated blood-brain barrier opening. *Theranostics* 2018; **8**: 2909–26. doi: https://doi.org/10.7150/thno.24911
75. Wu S-Y, Aurup C, Sanchez CS, Grondin J, Zheng W, Kamimura H, et al. Efficient blood-brain barrier opening in primates with neuronavigation-guided ultrasound and real-time acoustic mapping. *Sci Rep* 2018; **8**: 7978. doi: https://doi.org/10.1038/s41598-018-25904-9
76. Pouliopoulos AN, Burgess MT, Konofagou EE. Pulse inversion enhances the passive mapping of microbubble-based ultrasound therapy. *Appl Phys Lett* 2018; **113**: 044102. doi: https://doi.org/10.1063/1.5036516
77. Jones RM, O'Reilly MA, Hynynen K. Transcranial passive acoustic mapping with hemispherical sparse arrays using CT-based skull-specific aberration corrections: a simulation study. *Phys Med Biol* 2013; **58**: 4981–5005. doi: https://doi.org/10.1088/0031-9155/58/14/4981
78. Arvanitis CD, Clement GT, McDannold N. Transcranial assessment and visualization of acoustic cavitation: modeling and experimental validation. *IEEE Trans Med Imag* 2015; **34**: 1270–81. doi: https://doi.org/10.1109/TMI.2014.2383835
79. Jones RM, Hynynen K. Comparison of analytical and numerical approaches for CT-based aberration correction in transcranial passive acoustic imaging. *Phys Med Biol* 2016; **61**: 23–36. doi: https://doi.org/10.1088/0031-9155/61/1/23
80. Hynynen K. The threshold for thermally significant cavitation in dog's thigh muscle *in vivo*. *Ultrasound Med Biol* 1991; **17**: 157–69. doi: https://doi.org/10.1016/0301-5629(91)90123-E
81. Holland CK, Deng CX, Apfel RE, Alderman JL, Fernandez LA, Taylor KJW. Direct evidence of cavitation *in vivo* from diagnostic ultrasound. *Ultrasound Med Biol* 1996; **22**: 917–25. doi: https://doi.org/10.1016/0301-5629(96)00083-X
82. Feinstein SB, Shah PM, Bing RJ, Meerbaum S, Corday E, Chang B-L, et al. Microbubble dynamics visualized in the intact capillary circulation. *J Am Coll Cardiol* 1984; **4**: 595–600. doi: https://doi.org/10.1016/S0735-1097(84)80107-2
83. Miller D. Overview of experimental studies of biological effects of medical ultrasound caused by gas body activation and inertial cavitation. *Prog Biophys Mol Biol* 2007; **93**(1-3): 314–30. doi: https://doi.org/10.1016/j.pbiomolbio.2006.07.027
84. Stride E, Saffari N. Microbubble ultrasound contrast agents: A review. *Proc Inst Mech Eng H* 2003; **217**: 429–47. doi: https://doi.org/10.1243/09544110360729072
85. Leighton TG. *The acoustic bubble*. San Diego, CA, USA: Academic Press; 1994.
86. Lewin PA, Bjo/rno/ L. Acoustically induced shear stresses in the vicinity of microbubbles in tissue. *J Acoust Soc Am* 1982; **71**: 728–34. doi: https://doi.org/10.1121/1.387549
87. Chen H, Kreider W, Brayman AA, Bailey MR, Matula TJ. Blood vessel deformations on microsecond time scales by ultrasonic cavitation. *Phys Rev Lett* 2011; **106**: 034301. doi: https://doi.org/10.1103/PhysRevLett.106.034301
88. Caskey CF, Qin S, Dayton PA, Ferrara KW. Microbubble tunneling in gel phantoms. *J Acoust Soc Am* 2009; **125**: EL183–EL189. doi: https://doi.org/10.1121/1.3097679
89. Helfield B, Chen X, Watkins SC, Villanueva FS. Biophysical insight into mechanisms of sonoporation. *Proc Natl Acad Sci U S A* 2016; **113**: 9983–8. doi: https://doi.org/10.1073/pnas.1606915113
90. Sheikov N, McDannold N, Vykhodtseva N, Jolesz F, Hynynen K. Cellular mechanisms of the blood-brain barrier opening induced by ultrasound in presence of microbubbles. *Ultrasound Med Biol* 2004; **30**: 979–89. doi: https://doi.org/10.1016/j.ultrasmedbio.2004.04.010
91. Chomas JE, Dayton P, Allen J, Morgan K, Ferrara KW. Mechanisms of contrast agent destruction. *IEEE Trans Ultrason Ferroelectr Freq Control* 2001; **48**: 232–48. doi: https://doi.org/10.1109/58.896136
92. Borden MA, Kruse DE, Caskey CF, Zhao S, Dayton PA, Ferrara KW. Influence of lipid shell physicochemical properties on ultrasound-induced microbubble destruction. *IEEE Trans Ultrason Ferroelectr Freq Control* 2005; **52**: 1992–2002. doi: https://doi.org/10.1109/TUFFC.2005.1561668
93. Vykhodtseva N, McDannold N, Hynynen K. Induction of apoptosis *in vivo* in the rabbit brain with focused ultrasound and Optison®. *Ultrasound Med Biol* 2006; **32**: 1923–9. doi: https://doi.org/10.1016/j.ultrasmedbio.2006.06.026
94. Lele PP. Cavitation and its effects on organized mammalian tissues. In: Fry F. J, ed. *Ultrasound: its applications in medicine and biology*. Amsterdam, The Netherlands: Elsevier; 1978. pp. 737–41.
95. Neppiras EA. Subharmonic and other low-frequency emission from bubbles in sound-irradiated liquids. *J Acoust Soc Am* 1969; **46**(3B): 587–601. doi: https://doi.org/10.1121/1.1911735
96. Lauterborn W. Numerical investigation of nonlinear oscillations of gas bubbles in liquids. *J Acoust Soc Am* 1976; **59**: 283–93. doi: https://doi.org/10.1121/1.380884
97. Prosperetti A. A general derivation of the subharmonic threshold for non-linear bubble oscillations. *J Acoust Soc Am* 2013; **133**: 3719–26. doi: https://doi.org/10.1121/1.4802742
98. Sijl J, Dollet B, Overvelde M, Garbin V, Rozendal T, de Jong N, et al. Subharmonic behavior of phospholipid-coated ultrasound contrast agent microbubbles. *J Acoust Soc Am* 2010; **128**: 3239–52. doi: https://doi.org/10.1121/1.3493443
99. Faez T, Emmer M, Docter M, Sijl J, Versluis M, de Jong N. Characterizing the subharmonic response of phospholipid-coated microbubbles for carotid imaging. *Ultrasound Med Biol* 2011; **37**: 958–70. doi: https://doi.org/10.1016/j.ultrasmedbio.2011.02.017

100. Sijl J, Vos HJ, Rozendal T, de Jong N, Lohse D, Versluis M. Combined optical and acoustical detection of single microbubble dynamics. *J Acoust Soc Am* 2011; **130**: 3271–81. doi: https://doi.org/10.1121/1.3626155
101. Gateau J, Aubry JF, Pernot M, Fink M, Tanter M. Combined passive detection and ultrafast active imaging of cavitation events induced by short pulses of high-intensity ultrasound. *IEEE Trans Ultrason Ferroelectr Freq Control* 2011; **58**: 517–32. doi: https://doi.org/10.1109/TUFFC.2011.1836
102. Crake C, Brinker ST, Coviello CM, Livingstone MS, McDannold NJ. A dual-mode hemispherical sparse array for 3D passive acoustic mapping and skull localization within a clinical MRI guided focused ultrasound device. *Phys Med Biol* 2018; **63**: 065008. doi: https://doi.org/10.1088/1361-6560/aab0aa
103. Harris GR. Progress in medical ultrasound exposimetry. *IEEE Trans Ultrason Ferroelectr Freq Control* 2005; **52**: 717–36. doi: https://doi.org/10.1109/TUFFC.2005.1503960
104. Jeanmonod D, Werner B, Morel A, Michels L, Zadicario E, Schiff G, et al. Transcranial magnetic resonance imaging–guided focused ultrasound: noninvasive central lateral thalamotomy for chronic neuropathic pain. *Neurosurg Focus* 2012; **41**: E1. doi: https://doi.org/10.3171/2011.10.FOCUS11248
105. Sun T, Samiotaki G, Wang S, Acosta C, Chen CC, Konofagou EE. Acoustic cavitation-based monitoring of the reversibility and permeability of ultrasound-induced blood-brain barrier opening. *Phys Med Biol* 2015; **60**: 9079–94. doi: https://doi.org/10.1088/0031-9155/60/23/9079
106. Aryal M, Fischer K, Gentile C, Gitto S, Zhang YZ, McDannold N. Effects on P-glycoprotein expression after blood-brain barrier disruption using focused ultrasound and microbubbles. *PLoS One* 2017; **12**: e0166061. doi: https://doi.org/10.1371/journal.pone.0166061
107. Tsai C-H, Chen K-T, Lin Y-X, Lin Y-C, Chen W-S, Inserra C. Acoustic emission-feedback planar ultrasound system for localized blood–brain barrier opening monitoring. *J Med Biol Eng* 2018; **24**. doi: https://doi.org/10.1007/s40846-018-0406-x
108. Huang Y, Alkins R, Chapman M, Perry J, Sahgal A, Trudeau M. Initial experience in a pilot study of blood-brain barrier opening for chemo-drug delivery to brain tumors by MR-guided focused ultrasound. In: *ISMRM 24th Annual Meeting 2016*. Singapore; 2016. http://archive.ismrm.org/2016/0450.html.
109. Huang Y, Lipsman N, Meng Y, Bethune A, Lam B, Masellis M. Feasibility of blood-brain barrier opening in patients with Alzheimer's disease by MR-guided focused ultrasound. In: *ISMRM 26th Annual Meeting 2018*. France; 2018. https://www.ismrm.org/18/program_files/O82.htm.
110. Maimbourg G, Houdouin A, Santin M, Lehericy S, Tanter M, Aubry JF. Inside/outside the brain binary cavitation localization based on the lowpass filter effect of the skull on the harmonic content: a proof of concept study. *Phys Med Biol* 2018; **63**: 135012. doi: https://doi.org/10.1088/1361-6560/aaca21
111. Clement GT, White PJ, Hynynen K. Enhanced ultrasound transmission through the human skull using shear mode conversion. *J Acoust Soc Am* 2004; **115**: 1356–64. doi: https://doi.org/10.1121/1.1645610
112. Top CB, White PJ, McDannold NJ. Nonthermal ablation of deep brain targets: A simulation study on a large animal model. *Med Phys* 2016; **43**: 870–82. doi: https://doi.org/10.1118/1.4939809
113. Fry FJ, Kossoff G, Eggleton RC, Dunn F. Threshold ultrasonic dosages for structural changes in the mammalian brain. *J Acoust Soc Am* 1970; **48**(6B): 1413–7. doi: https://doi.org/10.1121/1.1912301
114. McDannold NJ, Vykhodtseva NI, Hynynen K. Microbubble contrast agent with focused ultrasound to create brain lesions at low power levels: MR imaging and histologic study in rabbits. *Radiology* 2006; **241**: 95–106. doi: https://doi.org/10.1148/radiol.2411051170
115. Arvanitis CD, Vykhodtseva N, Jolesz F, Livingstone M, McDannold N. Cavitation-enhanced nonthermal ablation in deep brain targets: feasibility in a large animal model. *J Neurosurg* 2016; **14**: 1450–9. doi: https://doi.org/10.3171/2015.4.JNS142862
116. Coleman AJ, Whitlock M, Leighton T, Saunders JE. The spatial distribution of cavitation induced acoustic emission, sonoluminescence and cell lysis in the field of a shock wave lithotripter. *Phys Med Biol* 1993; **38**: 1545–60. doi: https://doi.org/10.1088/0031-9155/38/11/001
117. Burns PN. Harmonic imaging with ultrasound contrast agents. *Clin Radiol* 1996; **51**: 50–5.
118. Simpson DH, Burns PN, Chin CT. Pulse inversion Doppler: a new method for detecting nonlinear echoes from microbubble contrast agents. *IEEE Trans Ultrason Ferroelectr Freq Control* 1999; **46**: 372–82. doi: https://doi.org/10.1109/58.753026
119. Du J, Liu D, Ebbini ES. Nonlinear Imaging of Microbubble Contrast Agent Using the Volterra Filter: *In Vivo* Results. *IEEE Trans Ultrason Ferroelectr Freq Control* 2006; **63**: 2069–81. doi: https://doi.org/10.1109/TUFFC.2016.2614430
120. Lucht B, Hubbell A, Hynynen K. Contrast-enhanced transcranial two-dimensional ultrasound imaging using shear-mode conversion at low frequency. *Ultrasound Med Biol* 2013; **39**: 332–44. doi: https://doi.org/10.1016/j.ultrasmedbio.2012.09.007
121. Korpel A. Acoustic imaging and holography. *IEEE Spectr* 1968; **5**: 45–52. doi: https://doi.org/10.1109/MSPEC.1968.5215380
122. Sato T, Nakamura Y, Sasaki K, Uemura K. Three dimensional passive acoustical imaging system using hemispherical array detectors. In: Metherell AF, ed. *Acoustical imaging*. Boston, MA: Springer; 1980. pp. 187–200.
123. Buckingham MJ, Berknout BV, Glegg SAL. Imaging the ocean with ambient noise. *Nature* 1992; **356**: 327–9. doi: https://doi.org/10.1038/356327a0
124. Kruger RA, Liu P, Fang YR, Appledorn CR. Photoacoustic ultrasound (PAUS)--reconstruction tomography. *Med Phys* 1995; **22**: 1605–9. doi: https://doi.org/10.1118/1.597429
125. Norton SJ, Won IJ. Time exposure acoustics. *IEEE Transactions on Geoscience and Remote Sensing* 2000; **38**: 1337–43. doi: https://doi.org/10.1109/36.843027
126. Farny CH, Holt RG, Roy RA. Temporal and spatial detection of HIFU-induced inertial and hot-vapor cavitation with a diagnostic ultrasound system. *Ultrasound Med Biol* 2009; **35**: 603–15. doi: https://doi.org/10.1016/j.ultrasmedbio.2008.09.025
127. Salgaonkar VA, Datta S, Holland CK, Mast TD. Passive cavitation imaging with ultrasound arrays. *J Acoust Soc Am* 2009; **126**: 3071–83. doi: https://doi.org/10.1121/1.3238260
128. Gyöngy M, Coussios CC. Passive spatial mapping of inertial cavitation during HIFU exposure. *IEEE Trans Biomed Eng* 2010; **57**: 48–56. doi: https://doi.org/10.1109/TBME.2009.2026907
129. Haworth KJ, Mast TD, Radhakrishnan K, Burgess MT, Kopechek JA, Huang S-L, et al. Passive imaging with pulsed ultrasound insonations. *J Acoust Soc Am* 2012; **132**: 544–53. doi: https://doi.org/10.1121/1.4728230
130. Choi JJ, Carlisle RC, Coviello C, Seymour L, Coussios C-C. Non-invasive and real-time passive acoustic mapping of ultrasound-mediated drug delivery. *Phys Med Biol* 2014;

59: 4861–77. doi: https://doi.org/10.1088/0031-9155/59/17/4861
131. Lu S, Shi A, Jing B, Du X, Wan M. Real-time monitoring of controllable cavitation erosion in a vessel phantom with passive acoustic mapping. *Ultrason Sonochem* 2017; **39**: 291–300. doi: https://doi.org/10.1016/j.ultsonch.2017.03.060
132. Acconcia CN, Jones RM, Goertz DE, O'Reilly MA, Hynynen K. Megahertz rate, volumetric imaging of bubble clouds in sonothrombolysis using a sparse hemispherical receiver array. *Phys Med Biol* 2017; **62**: L31–L40. doi: https://doi.org/10.1088/1361-6560/aa84d7
133. Jones RM, Hynynen K. Ultrafast three-dimensional imaging of contrast agent microbubble dynamics in vivo during pulsed ultrasound exposures in the brain. In: *International Symposium for Therapeutic Ultrasound*. USA; 2018.
134. O'Reilly MA, Hynynen K. A super-resolution ultrasound method for brain vascular mapping. *Med Phys* 2013; **40**: 110701. doi: https://doi.org/10.1118/1.4823762
135. Errico C, Pierre J, Pezet S, Desailly Y, Lenkei Z, Couture O, et al. Ultrafast ultrasound localization microscopy for deep super-resolution vascular imaging. *Nature* 2015; **527**: 499–502. doi: https://doi.org/10.1038/nature16066
136. Postert T, Federlein J, Przuntek H, Büttner T. Insufficient and absent acoustic temporal bone window: Potential and limitations of transcranial contrast-enhanced color-coded sonography and contrast-enhanced power-based sonography. *Ultrasound Med Biol* 1997; **23**: 857–62. doi: https://doi.org/10.1016/S0301-5629(97)00047-1
137. O'Reilly MA, Jones RM, Hynynen K. Investigating a method for non-invasive ultrasound aberration correction through the skull bone. *Proc SPIE Med Imag* 2014; **904013**.
138. Jones R, Deng L, Leung K, McMahon D, O'Reilly M, Hynynen K. Repeated hippocampal blood-brain barrier opening controlled via three-dimensional transcranial acoustic imaging: safety study in a porcine model. In: *IEEE International Ultrasonics Symposium*. USA; 2017. doi: https://doi.org/DOI: 10.1109/ULTSYM.2017.8091965
139. Liu H-L, Tsai C-H, Jan C-K, Chang H-Y, Huang S-M, Li M-L, et al. Design and implementation of a transmit/receive ultrasound phased array for brain applications. *IEEE Trans Ultrason Ferroelectr Freq Control* 2018; **65**: 1756–67. doi: https://doi.org/10.1109/TUFFC.2018.2855181
140. Molina CA, Ribo M, Rubiera M, Montaner J, Santamarina E, Delgado-Mederos R, et al. Microbubble administration accelerates clot lysis during continuous 2-MHz ultrasound monitoring in stroke patients treated with intravenous tissue plasminogen activator. *Stroke* 2006; **37**: 425–9. doi: https://doi.org/10.1161/01.STR.0000199064.94588.39
141. Schuster TG, Wei JT, Hendlin K, Jahnke R, Roberts WW. Histotripsy treatment of benign prostatic enlargement using the $Vort_x$ R_x system: initial human safety and efficacy outcomes. *Urology* 2018; **114**: 184–7. doi: https://doi.org/10.1016/j.urology.2017.12.033